Opposite quantum fluctuation effects on the vitrification of two atomic model liquids

Yang Zhou [1,2,*] Ali Eltareb [1,2] Gustavo E. Lopez,[3,4,†] and Nicolas Giovambattista [1,2,4,‡]

[1]*Department of Physics, Brooklyn College of the City University of New York, Brooklyn, New York 11210, USA*
[2]*Physics Department, The Graduate Center of the City University of New York, New York, New York 10016, USA*
[3]*Department of Chemistry, Lehman College of the City University of New York, Bronx, New York 10468, USA*
[4]*Chemistry Department, The Graduate Center of the City University of New York, New York, New York 10016, USA*

(Received 18 June 2026; accepted 8 October 2026; published 30 October 2026)

Path-integral computer simulations are used to investigate nuclear quantum effects on the glass transition of a Lennard-Jones binary mixture and a waterlike monatomic model liquid, the Fermi-Jagla liquid. As in previous studies, we find that introducing realistic atoms delocalization (nuclear quantum effects) suppresses atomic diffusivity in the Lennard-Jones binary mixture. Instead, nuclear quantum effects enhance the dynamics of the Fermi-Jagla liquid. Hence, nuclear quantum effects can either inhibit or promote the vitrification of atomic liquids depending on the atomic interactions. Notably, both systems exhibit qualitatively similar atoms delocalization and become less structured upon the inclusion of nuclear quantum effects, despite the divergent effects on their dynamics. A qualitative explanation of the different nuclear quantum effects on the dynamics of the Lennard-Jones binary mixture and Fermi-Jagla liquid is provided in terms of the features in the corresponding pair potential interactions. Our observations can be naturally interpreted through the potential energy landscape (PEL) formalism for quantum liquids. At a given temperature, introducing nuclear quantum effects forces the Lennard-Jones binary mixture to explore deeper regions of the PEL, where topographical features significantly affect the dynamics, while the Fermi-Jagla liquid is driven to explore higher regions of the PEL, where the PEL topography plays a secondary role. This is ultimately due to the opposite nuclear quantum effects on the PEL basins' *shape* (curvature) of the Lennard-Jones binary mixture and Fermi-Jagla liquid.

DOI: 10.1103/xfmw-ynv4

I. INTRODUCTION

The liquid-to-glass transition, a process characterized by a dramatic slowing down in dynamics without any major structural ordering, remains a central unsolved problem in condensed matter physics [1,2]. While most theoretical and computational studies have justifiably treated liquids classically, a complete understanding requires considering nuclear quantum effects (NQEs). These effects are crucial in low-temperature liquids composed of light elements, such as H_2 and He, and can be non-negligible in molecular systems containing hydrogen even near room temperature, as evidenced by the isotope effects in water [3,4]. The glassy state is not exclusive to atomic systems; it also manifests in quantum systems like electron liquids and spin ensembles [5–7].

The intuitive expectation is that NQEs—through zero-point energy and tunneling—should always enhance atoms/molecules' mobility, thereby fluidizing the system and suppressing glass formation. However, theoretical and computational studies on atomic liquids have fundamentally challenged this picture [8,9]. Specifically, path-integral simulations and quantum mode-coupling theory revealed a counterintuitive reentrant phenomenon in a quantum Lennard-Jones binary mixture (LJBM): Introducing weak or moderate quantum fluctuations slows the liquid's dynamics, pushing it deeper into a glassy state, while introducing sufficiently strong quantum fluctuations eventually restores the expected fluidizing effect [8,10]. Theoretical calculations based on a quantum replica method also show that NQEs slow down the dynamics of a Lennard-Jones liquid [9]. These studies raise fundamental questions: Do quantum fluctuations always suppress the dynamics of atomic liquids? If not, what physical principles determine whether quantum fluctuations promote or inhibit glass formation? More generally, how can we describe the role of quantum fluctuations in atomic liquids near their glass transition from a statistical-mechanics/thermodynamics perspective?

In this work, we address these questions and show that the influence of NQEs on the dynamics of atomic quantum liquids is dictated by the nature of the interatomic interactions. Specifically, we perform path-integral computer simulations of two distinct atomic liquids: (1) the canonical glass-former Kob-Andersen LJBM [11] and (2) the waterlike monatomic Fermi-Jagla liquid (FJL) [12,13]. We find that for weak and moderate quantum fluctuations, NQEs suppress the dynamics of the LJBM, consistent with previous work [8]. However,

*Contact author: yzhou4@gradcenter.cuny.edu
†Contact author: gustavo.lopez1@lehman.cuny.edu
‡Contact author: ngiovambattista@brooklyn.cuny.edu

Published by the American Physical Society under the terms of the Creative Commons Attribution 4.0 International license. Further distribution of this work must maintain attribution to the author(s) and the published article's title, journal citation, and DOI.

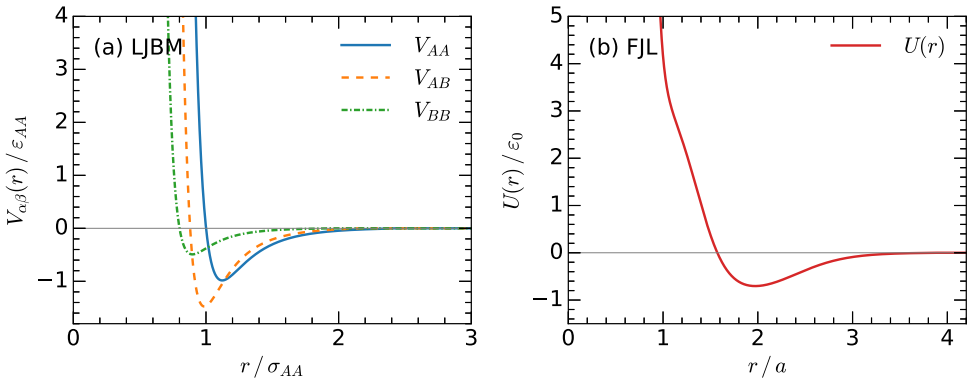


FIG. 1. (a) Pair interaction potentials between A-A, A-B, and B-B atoms in the LJBM studied [11]. (b) Pair interaction potential in the FJL. The Fermi-Jagla pair potential has a core-softened part for, approximately, particle separations $1 < r/a < 2$, and it is characterized by two length scales, $r/a \approx 1$ (hard-core radius) and $r/a \approx 2$ (close to the attractive potential energy minimum); see Ref. [13] for details.

NQEs markedly enhance the dynamics of the Fermi-Jagla liquid. Notably, despite this contrasting dynamical behavior, both liquids become less structured, with delocalized atoms, upon the inclusion of NQEs. The contrasting behaviors observed in the LJBM and FJL can be naturally understood within the potential energy landscape (PEL) framework recently extended to study quantum liquids [14,15]. At a given temperature, NQEs drive the LJBM to explore deeper regions of its PEL where the topography of the PEL becomes relevant and leads to slowing relaxation. Conversely, NQEs drive the FJL into higher-energy regions of its PEL where the topography of the PEL plays a secondary role, leading to faster atoms' mobility. Ultimately, the reported observations can be tracked down to the NQEs on the PEL basins' shape of the LJBM and FJL. We show that the contrasting effects of quantum fluctuations on the dynamics of the LJBM and FJL can be quantified by a single PEL variable, b, which may serve as a predictor for the (enhancing/suppressing) NQEs on the dynamics of atomic liquids.

Our motivation to study the FJL and LJBM is rather fundamental [8–10]. The LJBM is a prototypical well-studied, classical glass former that serves as an ideal model system to explore the role of quantum fluctuations (NQEs) in liquids and glasses. However, it is also possible that binary mixtures of isotopes or light elements, such as H_2 and He, could exhibit some of the properties observed in the quantum LJBMs studied (the corresponding LJ pair potential interactions may have to be reparametrized). Indeed, in a study of He, the pair interactions have been modeled through an LJ pair interaction potential [9]. Similarly, the FJL was proposed as a model liquid to reproduce many of the anomalous properties of water [12,16,17]. In particular, the NQEs observed in this model system [18,19], such as the role of quantum fluctuations in the FJL phase behavior and liquid-liquid critical point, have been like those observed in real water models [20,21]. In addition, we note that NQEs are not limited to H_2 and He, and can be observed in molecular systems at relatively high temperature [22], where isotope substitution effects (ultimately, due to NQEs) may be of interest. In this context, and depending on the application, computer simulations of molecular systems could benefit from the use of coarse-grained models. In this regard, LJ and effective potentials such as the Fermi-Jagla pair potential could be useful.

II. METHODS

Our results are based on ring-polymer molecular dynamics (RPMD) simulations [23] of the LJBM defined in Ref. [11] and the FJL defined in Ref. [13].

The LJBM defined in Ref. [11] is a well-established model liquid for studying glassy dynamics. It consists of N_A type-A atoms and N_B type-B atoms with $N_A/(N_A + N_B) = 0.80$. Pair interactions are given by the Lennard-Jones pair potential,

$$V_{\alpha\beta}(r) = 4\epsilon_{\alpha\beta}\left[\left(\frac{\sigma_{\alpha\beta}}{r}\right)^{12} - \left(\frac{\sigma_{\alpha\beta}}{r}\right)^{6}\right], \tag{1}$$

where $\alpha, \beta \in \{A, B\}$; see Fig. 1(a). We use standard reduced units where $\sigma_{AA} = 1.0$, $\epsilon_{AA} = 1.0$, and mass $m_A = m_B = 1.0$. The remaining interaction parameters are $\sigma_{BB} = 0.80$, $\sigma_{AB} = 0.88$, $\epsilon_{BB} = 0.5$, and $\epsilon_{AB} = 1.5$. The pair interactions are truncated and shifted at a cutoff distance $r_{c,\alpha\beta} = 2.5\sigma_{\alpha\beta}$. To ensure the forces are continuous functions of the interparticle distance, a switching function is applied between $r_{s,\alpha\beta} = 0.9r_{c,\alpha\beta}$ and $r_{c,\alpha\beta}$ as implemented in Ref. [24].

The FJL was introduced in Ref. [12] to model the properties of water in the liquid and glassy states. It can reproduce many of the anomalous properties of water, including the density maxima and the liquid-liquid and glass-glass transition [12]. The FJL is a monatomic liquid with pair interactions given by an isotropic, core-softened pair potential with two characteristic length scales ($r = a$ and $r \approx 2a$). Specifically,

$$U(r) = \epsilon_0\left[\frac{a^n}{r^n} + \frac{A_0}{1 + \exp\left[\frac{A_1}{A_0}(r/a - A_2)\right]} - \frac{B_0}{1 + \exp\left[\frac{B_1}{B_0}(r/a - B_2)\right]}\right] \tag{2}$$

with the parameters $\{a, \epsilon_0, A_{i=0,1,2}, B_{i=0,1,2}\}$ given in Refs. [12,13]; see Fig. 1(b). All properties are reported in reduced units where the energy unit is ϵ_0, the length unit is a, and the mass is $m = 1$. The Fermi-Jagla pair potential is truncated at $r_c = 4.0a$ and a switching function is applied for $r \in [3.6a, 4.0a]$ to ensure that the forces are continuous functions of the interparticle distance; see details in Ref. [13].

For both model liquids, RPMD simulations are performed for a system composed of $N = 1000$ atoms at a fixed density

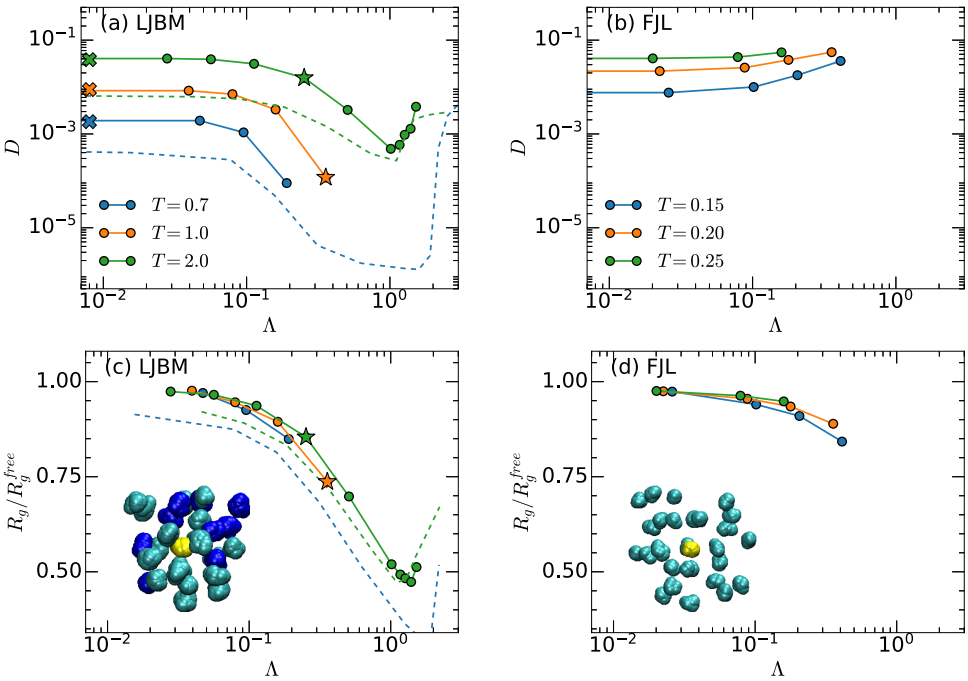


FIG. 2. Diffusion coefficient D (filled circles) as a function of the thermal de Broglie wavelength Λ for (a) the LJBM and (b) FJL. In panel (a), only type-A atoms are considered; however, similar results are obtained when considering only type-B atoms, or when including both type-A and type-B atoms in the system. With growing quantumness of the system (as quantified by an increasing Λ), the dynamics of the liquid slows down (LJBM) or speeds up (FJL), depending on the interatomic interactions. (c), (d) Radius of gyration $R_g(\Lambda)$ as a function of Λ evaluated from the same path-integral computer simulations included in panels (a) and (b). In all cases, $R_g(\Lambda)$ is normalized by the radius of gyration of the corresponding free atom, $R_g^{\text{free}}(\Lambda)$. Despite the different dynamics, for both liquids, the ratio $R_g(\Lambda)/R_g^{\text{free}}(\Lambda)$ decreases with increasing Λ in the weak and moderate quantum regimes (approximately $\Lambda < 0.5$). Dashed lines in panels (a) and (c) are taken from Refs. [8,10] at $T = 2.0$ (green dashed line) and $T = 0.7$ (blue dashed line); filled crosses in panel (a) mark the values of $D(T)$ for the *classical* LJBM ($\Lambda = 0$) reported in Ref. [11]. Filled stars in panels (a) and (c) mark the de Broglie thermal wavelength of He for two of the isotherms studied, $\Lambda_{\text{He}}(T) = \hbar/\sqrt{m_{\text{He}} k_B T}$; for each isotherm, Λ_{He} (stars) indicates approximately the largest physically realizable value of Λ for atomic liquids. Snapshots in panels (c) and (d) show an atom/ring polymer in yellow and its neighbors (LJBM: $T = 2.0$, $\Lambda \approx 0.25$, blue and cyan are type-A and type-B atoms; FJL: $T = 0.15$, $\Lambda \approx 0.21$).

($\rho = N/V = 1.2$ for the LJBM and $v = V/N = 2.2$ for the FJL) and different temperatures. In RPMD simulations, NQEs are incorporated by representing each atom as a ring polymer with n_b beads. In this study, we use $n_b \in [10, 256]$ (LJBM) and $n_b \in [10, 40]$ (FJL), depending on the temperature and quantumness of the system, so all studied thermodynamic and dynamical properties converge with respect to n_b. We also confirm that, at a given temperature, the value of n_b chosen satisfies the empirical relationship $n_b \geqslant \frac{\hbar\omega_{\max}}{k_B T}$, where $\omega_{\max}$ is the largest normal-mode frequency in the system [25]. Classical molecular dynamics (MD) simulations are performed by running RPMD simulations with $n_b = 1$. All RPMD/MD simulations were performed using the OpenMM (v7.3.0) software package where we modified the value of h as needed [24]. The temperature was controlled using a local path-integral Langevin equation thermostat with a stochastic collision frequency $\gamma = 0.1$. At each state point, we started the RPMD/MD simulations from a configuration obtained at high temperature. The system was equilibrated for a time $t_{\text{eq}} = 100\tau_\alpha$, where τ_α is the structural relaxation time (defined as the time needed for the atoms in the system to move over a distance equal to, approximately, the separation between nearest neighbors). Following equilibration, production runs were carried out for an additional time interval $t_{\text{prod}} = 100\tau_\alpha$ to calculate properties of the system and to collect configurations for PEL analysis. The simulation time step for the LJBM was $dt = 0.01$ (in reduced LJ units) for $T \leqslant 1.0$ and $dt = 0.001$ for $T \in (1.0, 5.0]$ (for all values of Λ considered). For the FJL, we used $dt = 0.0005$ (reduced Fermi-Jagla units) for all state points studied.

To elucidate the role of quantum mechanics in the dynamics of the LJBM and FJL, at each temperature studied, we performed a set of RPMD simulation using different values of the (reduced) Planck constant $\hbar$. Tuning $\hbar$ allows one to control the de Broglie thermal wavelength of the atoms $\Lambda = \hbar/\sqrt{mk_B T}$ and hence the atoms delocalization; see, e.g., Refs. [8,14,15,26]. The classical limit is recovered as $\Lambda \to 0$ and the liquid quantumness increases with growing Λ. In the case of the LJBM, we investigate de Broglie thermal wavelengths in the range $0 \leqslant \Lambda \leqslant 1.5$, where lengths are expressed in units of σ_{AA}, depending on the temperature considered. As discussed below, these values of Λ are comparable to the corresponding de Broglie's thermal wavelength for helium [Λ_{He}; see stars in Fig. 2(a)]. In the case of the FJL, we investigate de Broglie thermal wavelengths in the range $0 \leqslant \Lambda \leqslant 0.4$, where lengths are expressed in units of a, depending on the temperature considered.

To rationalize the contrasting NQEs on the dynamics of the LJBM and FJL, we employ the PEL formalism [27] extended to quantum liquids [15]. To analyze the PEL of the LJBM and FJL, we perform potential energy minimizations of ring-polymer configurations obtained during the production run. Specifically, for each T and Λ, we extract over 100 independent configurations (separated in time by $\Delta t = \tau_\alpha$) and calculate the corresponding potential energy minima, or inherent structures (ISs) [14,15]. Potential energy minimizations were performed using the L-BFGS-B algorithm as implemented in the `scipy.optimize` Python library [28]. The forces and potential energy required by the minimization algorithm were calculated using the OpenCL platform in OpenMM with double precision.

The local curvature of the PEL about the corresponding IS is quantified by the basin shape function,

$$\mathcal{S}(N, V, T, e_{\rm IS}) \approx \left\langle \ln\left[\prod_{j=1}^{3Nn_b}\left(\frac{\omega_j}{\omega_0}\right)\right]\right\rangle_{e_{\rm IS}}, \tag{3}$$

where $\{\omega_j\}_{j=1,2,\ldots,3Nn_b}$ are the normal mode frequencies of the ring-polymer system at the IS. The squared frequencies $\{\omega_j^2\}_{j=1,2,\ldots,3Nn_b}$ are the eigenvalues of the mass-weighted Hessian matrix and are evaluated following the procedure in Ref. [26]. Additional computational details for the IS calculation of the LJBM and FJL can be found in Refs. [26] and [15], respectively.

III. RESULTS

Figures 2(a) and 2(b) show the diffusion coefficient D of the atoms in the LJBM (type-A atoms) and FJL as a function of the thermal de Broglie wavelength Λ for selected isotherms. The temperature ranges explored in both cases are comparable; for example, the onset temperatures for these model liquids, as defined in Ref. [29], are $T_0 \approx 1.0$ (LJBM) [29] and $T_0 \approx 0.25$ (Fermi-Jagla) [13]. Consistent with Refs. [8,10] [dashed lines in Fig. 2(a)], we find that $D(\Lambda)$ for the LJBM exhibits a reentrant behavior, decreasing in the weak and moderate quantum regimes ($\Lambda < 0.5$–1.0) and increasing sharply in the strong quantum regime ($\Lambda > 1.0$). The stars on the isotherms in Fig. 2(a) mark the de Broglie thermal wavelength of He at the corresponding temperature and hence, the largest values of Λ that are physically feasible for atomic systems. In this physically accessible regime, introducing quantum fluctuations has the counterintuitive effect of slowing down the dynamics of the LJBM [8,10,30]. Surprisingly, we observe the opposite NQEs on the dynamics of the Fermi-Jagla liquid, where introducing quantumness in the system (increasing Λ) speeds up the liquid dynamics. The filled crosses in Fig. 2(a) indicate the values of D obtained from classical MD simulations of the LJBM (type-A atoms) reported in Ref. [11]. As expected, our RPMD simulation results converge to the classical values for $\Lambda \to 0$ (the results from Ref. [8] for the LJBM, dashed lines in Fig. 2(a), exhibit a small shift relative to our data and the classical values of Ref. [11]). The main point of Figs. 2(a) and 2(b) is that quantum fluctuations (in the physically accessible regime) can either increase or decrease the dynamics of atomic liquids at low temperatures, shifting its glass transition temperature to lower or higher temperatures, respectively, depending on the atomic interactions in the liquid. The results for the waterlike monatomic Fermi-Jagla liquid are consistent with path-integral simulations of water [31,32] and experiments [3] where the diffusion coefficient increases upon the D $\to$ H isotope substitution, as NQEs become more pronounced.

In Refs. [8,10], it is argued that the slowdown in the dynamics of the LJBM, in the weak and moderate quantum regimes [Fig. 2(a)], is due to the atoms delocalization and associated caging effects in the liquid. To explore this idea, included in Fig. 2(c) is the radius of gyration R_g of the LJBM atoms (type A) normalized by the corresponding value for the free atom $R_g^{\rm free}$. Consistent with Refs. [8,10], the ratio $R_g/R_g^{\rm free}$ decreases with increasing Λ in the weak and moderate quantum regimes, and is reentrant for very large values of Λ, following the behavior of $D(\Lambda)$ in Fig. 2(a). Surprisingly, our results for the Fermi-Jagla liquid [Fig. 2(d)] also show that the ratio $R_g/R_g^{\rm free}$ decreases monotonically with increasing Λ, following the opposite behavior of $D(\Lambda)$ in Fig. 2(b). It follows that the NQEs on the liquids dynamics are not necessarily related to the introduction of atoms delocalization (and associated caging effects).

To explore whether the opposite NQEs on the dynamics of the LJBM and FJL can be tracked down to particular structural changes, we include in Fig. 3 the bead-bead radial distribution function $g_{bb}(r)$ for the ring-polymer system associated with the atoms in the corresponding liquids. For both liquids, increasing the quantumness of the system leads to a less structured liquid: $g_{bb}(r)$ develops peaks that are progressively smaller in height and wider as Λ increases. Therefore, the opposite NQEs observed in the dynamics of the LJBM and FJL cannot be explained *solely* by a decrease in the liquid structure.

A closer comparison of the radial distribution functions in Figs. 3(a) and 3(b) reveals qualitatively distinct structural responses to NQEs in the LJBM and FJL. In the LJBM, increasing quantum fluctuations (increasing Λ) primarily reduces the height of the first peak in $g_{bb}(r)$ while slightly broadening it. This broadening reflects a modest expansion of the first solvation shell as quantum effects become significant. Notably, the peak positions remain largely unchanged indicating that NQEs do not substantially alter the solvation shell structure in LJBMs. In contrast, the FJL exhibits dramatic structural reorganization. As Λ increases, the first two maxima of $g_{bb}(r)$ approach each other and merge, with the first peak shifting to larger r values while the second peak shifts to smaller r. This results in a monotonic increase of $g_{bb}(r)$ across the range $1 < r < 2$, leading to the formation of a very broad first solvation shell. Classically (small Λ), the first solvation shell is localized at $r \approx 1$ and spans the range $1 < r < 1.4$; with increasing quantumness (large Λ), it shifts to $r \approx 1.4$ and extends across the distances $1 < r < 2$. These structural changes with increasing quantumness are related to the nature of the Fermi-Jagla pair potential; specifically, the beads' separations $1 < r < 2$ correspond to the core-softened part of the Fermi-Jagla potential [Fig. 1(b)]. In the range $1 < r < 2$, the bead-bead forces (within a replica) are repulsive, suggesting that such beads are transitioning between the hard-core distance ($r = 1$) and the Fermi-Jagla pair

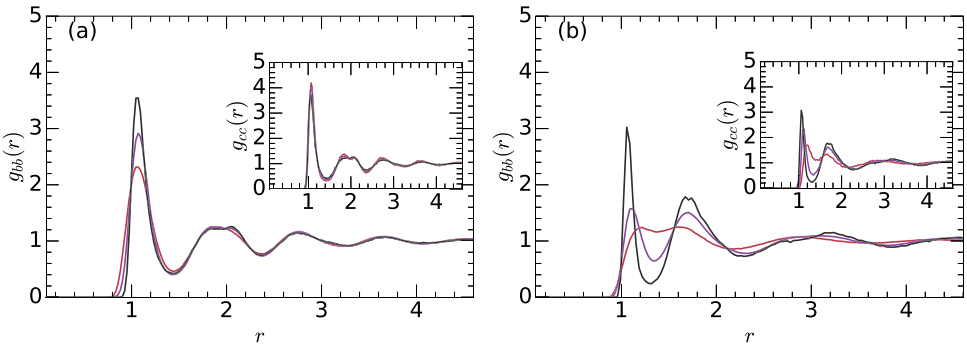


FIG. 3. Bead-bead radial distribution function of (a) the LJBM at $T = 0.70$ and (b) the FJL at $T = 0.15$ for different levels of quantumness (Λ). In both cases, including NQEs leads to a less structured liquid with a smaller first peak in the bead-bead radial distribution function, $g_{bb}(r)$. For comparison, included in the insets are the centroid-centroid radial distribution functions, $g_{cc}(r)$, of the LJBM and FJL. Black, purple, and crimson curves correspond, respectively, to $\Lambda = 0.047$, 0.190, and 0.427 for the LJBM, and to $\Lambda = 0.026$, 0.206, and 0.411 for the FJL.

potential minimum ($r \approx 2$). This dynamic mobility within a wide range of separations provides a plausible explanation to the enhanced diffusivity observed in FJL. Such a mechanism is absent in the LJBM.

IV. A DESCRIPTION BASED ON THE POTENTIAL ENERGY LANDSCAPE FORMALISM

Next, we show that the PEL approach [27,33], extended to the study of quantum liquids [14,15,26,31], provides a natural explanation of the opposite NQEs observed in the dynamics of the LJBM and FJL. To do so, we perform potential energy minimizations and obtain the local potential energy minima (or, ISs) sampled by the systems at different T and Λ. Figures 4(a) and 4(b) show the average IS energy as a function of Λ, $E_{\rm IS}(\Lambda)$, for the LJBM and FJL at selected temperatures. A comparison with Figs. 2(a) and 2(b) shows that, for both liquids, $E_{\rm IS}(\Lambda)$ mimics the behavior of $D(\Lambda)$. Indeed, even the reentrant behavior of $D(\Lambda)$ observed in Fig. 2(a) for the LJBM at $T = 2.0$ (green line) is present in the corresponding $E_{\rm IS}(\Lambda)$ [green line in Fig. 4(a)]. It follows that for physically accessible levels of quantumness [$\Lambda < \Lambda_{\rm He} \approx 0.3$–$0.5$; see stars in Fig. 2(a)], and at a given temperature, including NQEs drives the LJBM to explore deeper regions of the PEL while, instead, it drives the FJL to explore higher regions of the PEL. Since deeper regions of the PEL are associated with a slowdown in the dynamics of a liquid [29], the opposite NQEs in the dynamics of the LJBM and Fermi-Jagla liquid are naturally explained within the PEL formalism. We stress that for quantum liquids for which the ring polymers are collapsed at the ISs (as it is the case of the quantum Fermi-Jagla liquid and LJBM), the ISs are independent of the NQEs, and hence, the distributions of IS energies available in the PEL of the LJBM and FJL are Λ independent (see Refs. [15,26]).

To further expose the connection between the PEL and dynamics of the LJBM and FJL, included in Figs. 4(c) and 4(d) are the values of $E_{\rm IS}$ as a function of temperature for selected values of the Planck's constant h. The atoms' delocalization of liquids increases with increasing h [14,15,26,31] and hence so does the quantumness of the LJBM and FJL in Figs. 4(c) and 4(d). The main point of Figs. 4(c) and 4(d) is that, for the LJBM, the whole $E_{\rm IS}(T)$ curves shift toward higher temperatures implying that increasing the level of quantum fluctuations (as quantified by h) *effectively* shifts the PEL of the LJBM to higher temperatures. Instead, for the FJL, the $E_{\rm IS}(T)$ curves shift toward lower temperatures with increasing h, effectively shifting the PEL of the FJL to lower temperatures.

We also note that as found in numerous PEL studies, for all values of h, the $E_{\rm IS}(T)$ of the LJBM and FJL are constant at high temperatures and decrease rapidly at low temperatures as the system enters the so-called PEL-influenced regime [29]. The crossover between the high-temperature regime (where $E_{\rm IS}(T)$ is constant) and the PEL-influence regime occurs at the onset temperature T_0 [15,29]. Importantly, at $T < T_0$, the dynamics of the liquid slows down considerably upon cooling, as the liquid samples IS that are located in increasingly deeper regions of the PEL [14,15,26,31].

The contrasting NQEs on $D(\Lambda)$ and $E_{\rm IS}(\Lambda)$ of the LJBM and FJL [Figs. 2(a) and 2(b), and 4(a) and 4(b)] can, ultimately, be track down to the impact of quantum fluctuations on the topography of the corresponding PEL. To show this, we note that the PEL of the (classical and quantum) LJBM and FJL are Gaussian [15,26] implying that, at constant (N, V) [15],

$$E_{\rm IS}(T, \Lambda) \approx E_0 - \sigma^2(\tilde{b}(T, \Lambda) + \beta), \tag{4}$$

where E_0 and σ^2 are PEL variables independent of T and Λ [15,26]. In Eq. (4), $\tilde{b}(T, \Lambda) \equiv (\partial[\beta F_{\rm vib}(N, V, T, E_{\rm IS})]/\partial E_{\rm IS})_{N,V,T}$, where $F_{\rm vib}$ is the vibrational Helmholtz free energy of the liquid [15,31] that depends only on the shape of the PEL basins with energy $E_{\rm IS}$ about the corresponding IS [15]. It follows from Eq. (4) that altering the quantumness of the LJBM and FJL affects $E_{\rm IS}(T)$ solely through the PEL variable $\tilde{b}$.

If the PEL of the system of interest is harmonic, with parabolic (quadratic) basins about the IS, then $\tilde{b}$ reduces to the PEL variable $b \equiv (\partial \mathcal{S}/\partial E_{\rm IS})_{N,V,T}$ that is commonly used in PEL studies of liquids [34]. Here, $\mathcal{S} = \mathcal{S}(N, V, T, E_{\rm IS})$ is the basin shape function [34], a quantity that depends solely on the eigenvalues of the mass-weighted Hessian matrix of the system at the IS sampled by the system at the working conditions (N, V, T), and hence, it quantifies the curvature of the PEL basins about the corresponding IS [15]. The procedures to calculate the PEL variable b, as well as the associated basin shape function $\mathcal{S}$, are described in detail

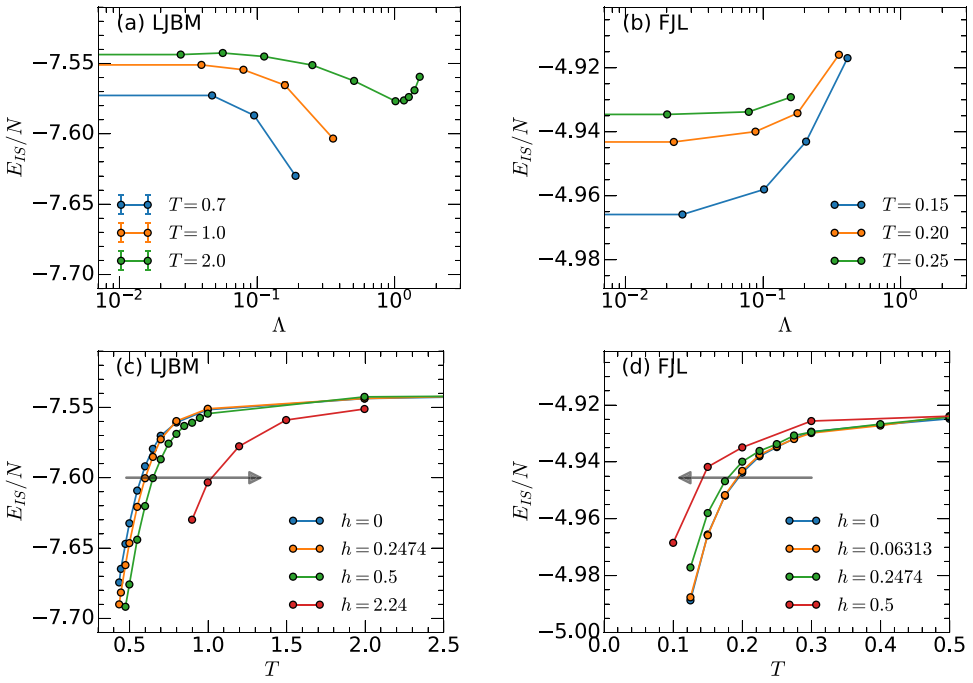


FIG. 4. Average inherent-structure energy, $E_{\rm IS}$, sampled by the LJBM and FJL. (a), (b) $E_{\rm IS}$ as a function of Λ from path-integral simulations at fixed temperatures. For physically accessible levels of quantumness ($\Lambda < 0.3-0.5$), the $E_{\rm IS}$ of the LJBM decreases with increasing Λ; i.e., introducing NQEs drives the LJBM to explore deeper regions in the PEL. Instead, NQEs drive the FJL to explore higher regions of the PEL (higher IS energies). For both liquids, $E_{\rm IS}(\Lambda)$ mimics the behavior of $D(\Lambda)$ in Figs. 2(a) and 2(b). (c), (d) $E_{\rm IS}$ as a function of T from path-integral simulations with modified values of the Planck's constant h. At a given temperature, the delocalization of the atoms increases with increasing h since $\Lambda = \hbar/\sqrt{mk_BT}$. Consistent with panels (a) and (b), increasing h shifts the $E_{\rm IS}(T)$ curves of the LJBM (FJL) toward higher (lower) temperatures (see arrows).

in Ref. [26]. If anharmonic contributions are necessary, then $\tilde{b} = b - \sigma^2\tilde{B}_1$, where the last term of this expression includes contributions to the system due to anharmonic contributions; see Ref. [26] for details. Usually, anharmonic contributions for $E_{\rm IS}(T)$ are small or negligible [15,26,31,32], and hence, $\tilde{b}(T, \Lambda) \approx b(T, \Lambda)$ to a first-order approximation (for a given Λ). Figure 5 shows the calculated $b(\Lambda)$ for the LJBM and FJL at selected temperatures. For the LJBM system, $b(\Lambda) > 0$ and *increases* with increasing quantumness (Λ), consistent with the corresponding shift of $E_{\rm IS}(T)$ to higher temperatures [Eq. (4) and Fig. 4(c)]. In stark contrast, for the FJL, $b(\Lambda) < 0$ and *decreases* with increasing Λ, consistent with the shift in the corresponding $E_{\rm IS}(T)$ to lower temperatures [Eq. (4) and Fig. 4(d)]. Overall, our results indicate that the opposite NQEs on the dynamics of the LJBM and FJL are related to the manner in which NQEs affect the shape of the basins in the PEL of these model liquids: A positive $(\partial b/\partial\Lambda)_T$ signals NQE-enhanced vitrification, while a negative $(\partial b/\partial\Lambda)_T$ signals NQE-suppressed vitrification.

V. SUMMARY AND DISCUSSION

In conclusion, our path-integral simulations of the LJBM and FJL indicate that the effects of quantum fluctuations (NQEs) on the dynamics and glass transition temperature of atomic liquids are not universal but depend on the specific interatomic interactions [Figs. 2(a) and 2(b)]. NQEs on the

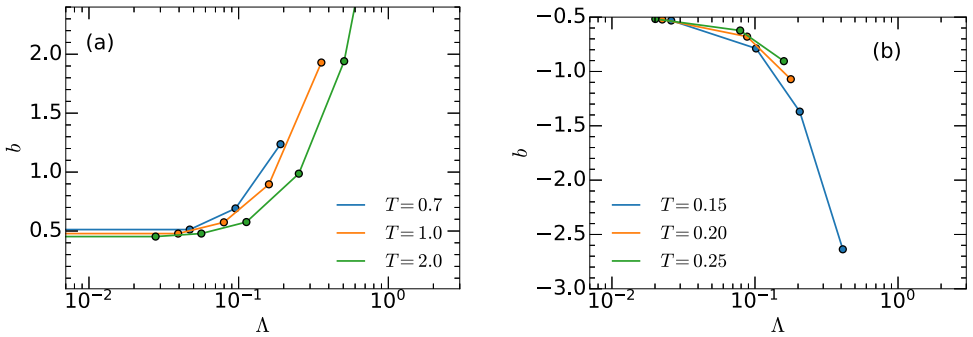


FIG. 5. PEL variable b as a function of the de Broglie thermal wavelength, Λ, at selected temperatures. (a) For the LJBM, $b > 0$ and increases with increasing Λ, while (b) for the FJL, $b < 0$ and decreases with increasing Λ. The opposite NQE on the topography of the PEL, as quantified by b, correlates with the contrasting NQE on the dynamics of the LJBM and FJL.

atoms delocalization of the LJBM and FJL are qualitatively similar [Figs. 2(c) and 2(d)] and hence cannot explain the contrasting NQEs on the dynamics of these liquids. Similarly, both liquids become less structured as NQEs are included (Fig. 3). Our results based on the PEL formalism indicate that, at a given temperature, the introduction of quantum fluctuations drives the studied liquids to explore different regions of the corresponding PEL (Fig. 4). In the case of the LJBM, introducing NQEs drives the system to explore ISs located in deeper regions of the PEL, which explains the slowdown of the atoms' mobility; in the case of the FJL, introducing NQEs drives the system to explore ISs located in higher regions of the PEL, which explains the speedup of the atoms' mobility. Path-integral computer simulations suggest that the contrasting NQEs on the dynamics of these systems are, ultimately, related to the opposite NQEs on the PEL basins' *shape* (curvature) of the LJBM and FJL, providing a topographic explanation of the contrasting dynamical behavior of these liquids. Our results suggest that the *dependence* of the PEL parameter b on Λ may be a good predictor of the NQEs on the liquid dynamics and glass transition temperature (Fig. 5). Specifically, including quantum fluctuations is expected to shift the glass transition temperature to higher [lower] temperatures for a liquid with $(\partial b/\partial \Lambda)_T > 0$ $[(\partial b/\partial \Lambda)_T < 0]$.

ACKNOWLEDGMENTS

This work was supported by the NSF-CREST Center for Interface Design and Engineered Assembly of Low Dimensional Systems (IDEALS), NSF Grant No. HRD-1547380. This work was also supported by the Advanced Cyberinfrastructure Coordination Ecosystem: Services & Support (ACCESS) program, which is supported by the National Science Foundation Grants No. 2138259, No. 2138286, No. 2138307, No. 2137603, and No. 2138296. Y.Z. is thankful for financial support from The Grace Spruch '47 Fund from the Physics Department of Brooklyn College, CUNY.

DATA AVAILABILITY

There are no publicly available research data or software supporting this manuscript. Requests for further information or data should be sent to the authors.

[1] P. G. Debenedetti and F. H. Stillinger, Supercooled liquids and the glass transition, Nature (London) **410**, 259 (2001).

[2] L. Berthier and G. Biroli, Theoretical perspective on the glass transition and amorphous materials, Rev. Mod. Phys. **83**, 587 (2011).

[3] C. Gainaru, A. L. Agapov, V. Fuentes-Landete, K. Amann-Winkel, H. Nelson, K. W. Köster, A. I. Kolesnikov, V. N. Novikov, R. Richert, R. Böhmer, T. Loerting, and A. P. Sokolov, Anomalously large isotope effect in the glass transition of water, Proc. Natl. Acad. Sci. USA **111**, 17402 (2014).

[4] M. Ceriotti, W. Fang, P. G. Kusalik, R. H. McKenzie, A. Michaelides, M. A. Morales, and T. E. Markland, Nuclear quantum effects in water and aqueous systems: Experiment, theory, and current challenges, Chem. Rev. **116**, 7529 (2016).

[5] A. Amir, Y. Oreg, and Y. Imry, Slow relaxations and aging in the electron glass, Phys. Rev. Lett. **103**, 126403 (2009).

[6] W. Wu, B. Ellman, T. F. Rosenbaum, G. Aeppli, and D. H. Reich, From classical to quantum glass, Phys. Rev. Lett. **67**, 2076 (1991).

[7] A. D. King, J. Raymond, T. Lanting, R. Harris, A. Zucca, F. Altomare, A. J. Berkley, K. Boothby, S. Ejtemaee, C. Enderud, *et al.*, Quantum critical dynamics in a 5,000-qubit programmable spin glass, Nature (London) **617**, 61 (2023).

[8] T. E. Markland, J. A. Morrone, B. J. Berne, K. Miyazaki, E. Rabani, and D. R. Reichman, Quantum fluctuations can promote or inhibit glassformation, Nat. Phys. **7**, 134 (2011).

[9] G. Biroli and F. Zamponi, A tentative replica theory of glassy helium 4, J. Low Temp. Phys. **168**, 101 (2012).

[10] T. E. Markland, J. A. Morrone, K. Miyazaki, B. J. Berne, D. R. Reichman, and E. Rabani, Theory and simulations of quantum glass forming liquids, J. Chem. Phys. **136**, 074511 (2012).

[11] W. Kob and H. C. Andersen, Testing mode-coupling theory for a supercooled binary Lennard-Jones mixture I: The van Hove correlation function, Phys. Rev. E **51**, 4626 (1995).

[12] J. Y. Abraham, S. V. Buldyrev, and N. Giovambattista, Liquid and glass polymorphism in a monatomic system with isotropic, smooth pair interactions, J. Phys. Chem. B **115**, 14229 (2011).

[13] G. Sun, L. Xu, and N. Giovambattista, Relationship between the potential energy landscape and the dynamic crossover in a water-like monatomic liquid with a liquid-liquid phase transition, J. Chem. Phys. **146**, 014503 (2017).

[14] N. Giovambattista and G. E. Lopez, Potential energy landscape formalism for quantum liquids, Phys. Rev. Res. **2**, 043441 (2020).

[15] Y. Zhou, G. E. Lopez, and N. Giovambattista, The harmonic and Gaussian approximations in the potential energy landscape formalism for quantum liquids, J. Chem. Theory Comput. **20**, 1847 (2024).

[16] L. Xu, S. V. Buldyrev, N. Giovambattista, and H. E. Stanley, Liquid-liquid phase transition and glass transition in a monoatomic model system, Int. J. Mol. Sci. **11**, 5184 (2010).

[17] N. Giovambattista, The liquid-liquid phase transition, anomalous properties, and glass behavior of polymorphic liquids, in *Advances in Chemical Physics*, edited by H. E. Stanley, 1st ed. (Wiley, Hoboken, New Jersey, 2013), Vol. 152, pp. 113–138.

[18] B. Nguyen, G. E. Lopez, and N. Giovambattista, Nuclear quantum effects on the liquid–liquid phase transition of a water-like monatomic liquid, Phys. Chem. Chem. Phys. **20**, 8210 (2018).

[19] A. Eltareb, G. E. Lopez, and N. Giovambattista, Nuclear quantum effects on the dynamics and glass behavior of a monatomic liquid with two liquid states, J. Chem. Phys. **156**, 204502 (2022).

[20] A. Eltareb, G. E. Lopez, and N. Giovambattista, Nuclear quantum effects on the thermodynamic, structural, and dynamical properties of water, Phys. Chem. Chem. Phys. **23**, 6914 (2021).

[21] A. Eltareb, G. E. Lopez, and N. Giovambattista, Nuclear quantum effects on the equation of state of water: Insights from the potential energy landscape formalism, J. Chem. Theory Comput. **22** 3208 (2026).

[22] B. E. Ugur and M. A. Webb, Nuclear quantum effects in molecular liquids across chemical space, Nat. Commun. **16**, 5786 (2025).

[23] I. R. Craig and D. E. Manolopoulos, Quantum statistics and classical mechanics: Real time correlation functions from ring polymer molecular dynamics, J. Chem. Phys. **121**, 3368 (2004).

[24] P. Eastman, J. Swails, J. D. Chodera, R. T. McGibbon, Y. Zhao, K. A. Beauchamp, L.-P. Wang, A. C. Simmonett, M. P. Harrigan, C. D. Stern, R. P. Wiewiora, B. R. Brooks, and V. S. Pande, OpenMM 7: Rapid development of high performance algorithms for molecular dynamics, PLoS Comput. Biol. **13**, e1005659 (2017).

[25] C. P. Herrero and R. Ramírez, Path-integral simulation of solids, J. Phys.: Condens. Matter **26**, 233201 (2014).

[26] Y. Zhou, A. Eltareb, G. E. Lopez, and N. Giovambattista, Configurational entropy and Adam-Gibbs relation for quantum liquids, Nat. Commun. **17**, 4843 (2026).

[27] F. H. Stillinger, *Energy Landscapes, Inherent Structures, and Condensed-Matter Phenomena* (Princeton University Press, Princeton, New Jersey, 2015).

[28] P. Virtanen, R. Gommers, T. E. Oliphant, M. Haberland, T. Reddy, D. Cournapeau, E. Burovski, P. Peterson, W. Weckesser, J. Bright, *et al.*, SciPy 1.0: Fundamental algorithms for scientific computing in Python, Nat. Methods **17**, 261 (2020).

[29] S. Sastry, P. G. Debenedetti, and F. H. Stillinger, Signatures of distinct dynamical regimes in the energy landscape of a glass-forming liquid, Nature (London) **393**, 554 (1998).

[30] F. Zamponi, Quantum glass forging, Nat. Phys. **7**, 99 (2011).

[31] A. Eltareb, Y. Zhou, G. E. Lopez, and N. Giovambattista, Potential energy landscape formalism for quantum molecular liquids, Commun. Chem. **7**, 289 (2024).

[32] A. Eltareb, G. E. Lopez, and N. Giovambattista, Isotope-substitution effects on the thermodynamic, dynamic, and structural properties of water: H_2O, HDO, D_2O, and T_2O, J. Phys. Chem. B **129**, 6886 (2025).

[33] F. H. Stillinger and T. A. Weber, Hidden structure in liquids, Phys. Rev. A **25**, 978 (1982).

[34] F. Sciortino, Potential energy landscape description of supercooled liquids and glasses, J. Stat. Mech. (2005) P05015.